



ELSEVIER

Contents lists available at ScienceDirect

# Polymer Degradation and Stability

journal homepage: [www.elsevier.com/locate/polydegstab](http://www.elsevier.com/locate/polydegstab)

## EVA-layered double hydroxide (nano)composites: Mechanism of fire retardancy

Xiaolan Wang<sup>a</sup>, Rajendra Rathore<sup>b</sup>, Ponusa Songtipya<sup>c,d</sup>, Maria del Mar Jimenez-Gasco<sup>d</sup>, Evangelos Manias<sup>c</sup>, Charles A. Wilkie<sup>a,\*</sup>

<sup>a</sup> Department of Chemistry and Fire Retardant Research Facility, Marquette University, Milwaukee, WI, USA

<sup>b</sup> Department of Chemistry, Marquette University, Milwaukee, WI, USA

<sup>c</sup> Polymer Nanostructures – Lab Center for the Study of Polymeric Systems, and Department of Materials Science & Engineering, Penn State University, University Park, PA, USA

<sup>d</sup> Plant Pathology Department, Penn State University, University Park, PA, USA

### ARTICLE INFO

#### Article history:

Received 30 January 2010

Received in revised form

4 March 2010

Accepted 12 March 2010

Available online 27 March 2010

#### Keywords:

EVA

TGA/FTIR/MS

Fire retardancy

Cone calorimetry

### ABSTRACT

Composites of ethylene–vinyl acetate copolymer with two different layered double hydroxides have been obtained by melt blending and these have been characterized by X-ray diffraction, transmission electron microscopy, thermogravimetric analysis, thermogravimetric analysis connected to mass spectroscopy and cone calorimetry. There is some small difference in dispersion between the zinc-containing and the magnesium-containing layered double hydroxides in EVA, but both these are microcomposites with good dispersion at the micrometer level and relatively poor dispersion at the nanometer level. There is a good reduction in the peak heat release rate at 10% LDH loading. In addition to chain stripping, which involves the simultaneous loss of both acetate and a hydrogen atom, forming acetic acid, and the formation of poly(ethylene-co-acetylene), side chain fragmentation of the acetate group also occurs and may be the dominant pathway of thermal degradation in the first step. The presence of the LDH causes acetone, rather than acetic acid, to be evolved in the initial step of the degradation.

© 2010 Elsevier Ltd. All rights reserved.

### 1. Introduction

The utility of polymer–clay nanocomposites in fire retardancy has been well-established. Depending on the polymer, one can observe a reduction in the peak heat release rate of up to 60%. The process by which this fire retardant character occurs upon the addition of a nano-dimensional inorganic filler material (typically montmorillonite clay (MMT)) has been probed by several groups and the consensus seems to be that a filler-promoted barrier to both mass and thermal transport is formed [1]. Careful systematic studies have further refined this underlying mechanism and revealed that the barrier does not necessarily have to rise to the surface; the clay particles can function as a barrier wherever they are within the polymer through a process that has been termed nano-confinement [2]. In this process, when a degradation event occurs and the degrading radicals are momentarily confined, an increased number of radical recombination reactions occur as a result, leading to the formation of a new polymer which must subsequently degrade. The net result of this is that the time for complete degradation is lengthened and so the heat release is spread out over time; a correlation has been seen between the

degradation pathway of the polymer and the reduction in the peak heat release rate [3]. Essentially, the reduction in the peak heat release rate is large when polymers degrade by random scission but not as large when end chain unzipping is the mechanism of degradation. This can also be seen through a change in the product distribution.

According to this mechanism, the underlying important requirement is that the radicals remain confined by the fillers for a time, thus, it is not important whether the nanocomposite has an intercalated or an exfoliated morphology, as long as there exists some nanoscale dispersion, since in either case the radicals will be effectively confined. While there is not yet a complete understanding of the process by which MMT functions in fire retardancy for each polymer, enough is known so that one can use this information to begin to understand how other nanoscale materials may function as fire retardants.

Two other nano-dimensional materials that have been used for fire retardancy are carbon nanotubes (CNT) and layered double hydroxides (LDH). Carbon nanotubes are effective at quite low amounts, for example, for single wall nanotubes in poly(methyl methacrylate) (PMMA), good fire retardant efficacy is seen at 0.2% CNT levels. The aspect ratio of the CNT is very important with higher aspect ratios yielding better fire retardancy [4]. With CNT, there is a large reduction in the peak heat release rate but no change in the product distribution which suggests that fire retardancy of

\* Corresponding author.

E-mail address: [charles.wilkie@marquette.edu](mailto:charles.wilkie@marquette.edu) (C.A. Wilkie).

CNT nanocomposite follow a pathway which is different from that of MMT systems [5,6]

The family of layered double hydroxides (LDH) are new materials as fire retardant additives. Interest in these LDHs developed after Zammarrano et al. showed that the addition of an LDH to polyamide 6 gave enhanced fire retardancy [7]. The situation with LDHs is rather poorly understood, since in contrast to MMT layered silicates, there is a substantial reduction in the PHRR even for systems in which the LDHs are not dispersed at the nanometer level [8] (with MMT, for example, there is typically no reduction in PHRR unless there is good nano-dispersion of the fillers). In previous work [6], we suggested, as a tentative notion, that if an LDH is dispersed at the nanometer level in a polymer, there may be changes in the degradation products but when the LDH is not nano-dispersed, the products are not changed.

The purpose of this work is to investigate EVA-LDH (nano) composites to further determine if the presence of the LDH has an effect on the degradation products with the ultimate goal to develop an understanding of the process by which LDHs can influence the fire retardancy of polymers. In previous work from these laboratories, we have shown that a ZnAl LDH interacts better with polypropylene and polyethylene than does a MgAl LDH. An additional objective in this study was to investigate the interaction of EVA with both the zinc-containing and the magnesium-containing LDHs.

## 2. Experimental

### 2.1. Materials

The materials used in the synthesis of oleate intercalated layered double hydroxides included: zinc nitrate hexahydrate (98%), magnesium nitrate hexahydrate, aluminum nitrate non-hydrate (98%) and sodium hydroxide, all obtained from the Aldrich Chemical Company and used as received; sodium oleate (J.T. Baker), and ethylene–vinyl acetate copolymer (EVA), 18% vinyl acetate, provided by ExxonMobil.

### 2.2. Preparation of the oleate LDHs

The oleate LDHs were synthesized using the co-precipitation method [9] under an  $N_2$  atmosphere in order to exclude carbon dioxide, which would lead to the formation of carbonate-containing LDHs. Typically, 1000 ml distilled water was boiled for 1 h while purging with nitrogen, then cooled to room temperature and transferred to a 3000 ml three-neck flask under a flow of nitrogen. A 0.1 mol portion of sodium oleate was added to the flask, and the mixture was stirred until the sodium oleate completely dissolved. In a second beaker, a solution of  $Mg(NO_3)_2 \cdot 6H_2O$  (0.2 mol) (or  $Zn(NO_3)_2 \cdot 6H_2O$ , 0.2 mol) and  $Al(NO_3)_3 \cdot 9H_2O$  (0.1 mol) in deionized and decarbonated water (500 ml) was prepared and then slowly added dropwise to the stirred sodium oleate solution at room temperature under a nitrogen atmosphere. The pH was maintained at 10.0 by the addition of 1 M sodium hydroxide solution. The resulting slurry was aged for 24 h at 70 °C, then washed several times with deionized and decarbonated water before drying in a vacuum oven at 70 °C.

### 2.3. Preparation of the polymer composites

EVA/LDH composites were prepared by melt blending in a Brabender mixer. The requisite amounts of EVA copolymer and the LDH were combined in a beaker and stirred, then transferred to the Brabender Plasticorder at a temperature of 130 °C and a screw speed of 60 rpm. The EVA/LDH composites were prepared at

loadings of 3%, 5% or 10% of the LDH. The time of blending was a variable; times of 1, 5 and 15 min were used to see how the time of blending effected dispersion. An unfilled reference sample of EVA was also subjected to the same process to serve as a reference.

### 2.4. Instrumentation

The powder X-ray diffraction measurements (PXRD) were performed using a Rigaku Miniflex II desktop X-ray diffractometer with a  $Cu(K\alpha)$  source,  $\lambda = 1.54078 \text{ \AA}$ ; data acquisition used a scan speed of  $2^\circ/\text{min}$  at a sampling width of  $0.020^\circ$  over a  $2\theta$  range from 2 to  $10^\circ$ . Bright field transmission electron microscopy (TEM) was performed on a JEOL 1200 EXII microscope equipped with a Tietz F224 digital camera and operated at an accelerating voltage of 80 kV. Sections of the nanocomposites were obtained with a Leica Ultracut UCT microtome, equipped with a diamond knife and sectioning was carried out at temperatures below the  $T_g$  of EVA, using liquid nitrogen to cool the composites within the microtome. The sections were transferred to carbon-coated copper grids (200-mesh) with or without a carbon lace, and imaged without any heavy metal staining. FTIR analyses were carried out on a Nicolet Magna-IR 560 spectrometer operated at  $1 \text{ cm}^{-1}$  resolution in the 400–4000  $\text{cm}^{-1}$  region using the KBr method. Thermogravimetric analyses (TGA) were performed on a SDT2960 (TA Instruments) at the 15 mg maximum scale under a air atmosphere with a scan rate of  $20^\circ\text{C}/\text{min}$ . Temperature is reproducible to  $\pm 3^\circ$  and mass to  $\pm 0.2\%$ ; all samples were run in duplicate and the average values are reported. TGA–FTIR–MS data was obtained using a Netzsch TG-209 F1 interfaced to a Netzsch QMS 403C mass spectrometer and a Bruker tensor 27 Fourier transform infrared spectrometer with an MCT detector. The transfer lines were maintained at 200 °C to prevent condensation of the evolved products. The TGA was ramped at  $20^\circ/\text{min}$  from room temperature to 800 °C and all samples were run in duplicate. Cone calorimeter measurements were performed on an Atlas CONE-2 using a cone shaped heater at an incident flux of  $35 \text{ KW}/\text{m}^2$ , according to ASTM E1354. The exhaust flow was set at 24 L/sec and the spark was continuous for 10 s until the specimen was ignited. The specimens were prepared by compression molding, with the weight of about 30 g, and dimensions of  $3 \times 100 \times 100 \text{ mm}^3$ . The results of cone calorimeter are reproducible to within about  $\pm 10\%$ , which is based on the many thousands of samples that have been run.

## 3. Results and discussion

### 3.1. Morphological characterization of the LDHs

Fig. 1 provides the XRD patterns of magnesium aluminum layered double hydroxide intercalated with oleate anion (MgAlO-LDH) and zinc aluminum layered double hydroxide intercalated with oleate anion (ZnAlO-LDH). For MgAlO-LDH, the strongest peak in the XRD pattern appears at  $2\theta = 2.72^\circ$ , corresponding to a basal spacing of 3.25 nm, and an interlayer spacing of 2.77 nm, which is obtained by subtracting 0.48 nm, the thickness of the brucitic layer [10]. The strongest peak for ZnAlO-LDH is at  $2\theta = 2.56^\circ$ , corresponding to a basal spacing of 3.45 nm and an interlayer spacing of 2.97 nm, about 0.2 nm larger than for MgAl. The basal spacing in the parent MgAl– $NO_3$  is 0.89 nm [8b]; the large increase in basal spacing confirms that oleate has been inserted into the gallery space of the LDH. The observation of three higher order diffraction peaks is also an indication that intercalation has occurred and that the LDH is fairly crystalline.

Additional proof of intercalation of the oleate ion comes from infrared spectroscopy. The FTIR spectra of MgAlO-LDH and ZnAlO-LDH are similar (Fig. 2). The strong and broad absorption

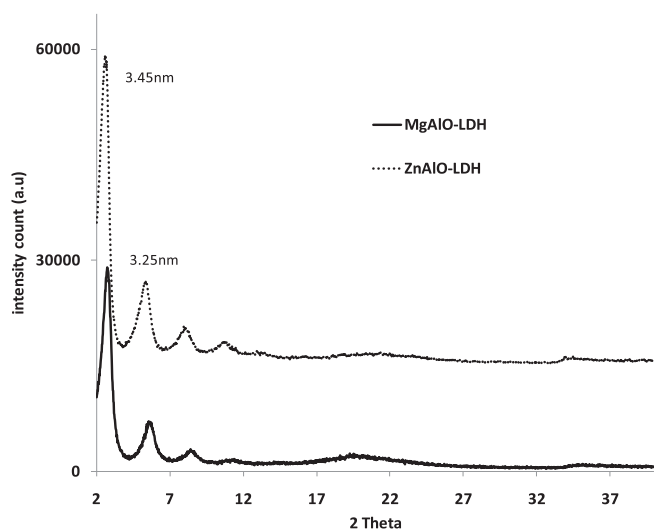


Fig. 1. XRD traces of MgAlO and ZnAlO LDHs.

peak at  $3408\text{ cm}^{-1}$  corresponds to the stretching vibration of  $-\text{OH}$ ; the peaks at  $3010\text{ cm}^{-1}$  and at  $2920\text{ cm}^{-1}$  are associated with the  $\text{C}-\text{H}$  stretching vibrations for the  $\text{sp}^2$  and  $\text{sp}^3$  carbons of the oleate anion, respectively. The peak due to the  $\text{C}=\text{C}$  stretching vibration of the oleate anion appears at  $1650\text{ cm}^{-1}$ . The presence of peaks at  $1550\text{ cm}^{-1}$  and  $1460\text{ cm}^{-1}$  are assigned to the asymmetric and symmetric stretching vibration for  $\text{RCOO}^-$ , respectively, of the oleate anion. The band at  $1410\text{ cm}^{-1}$  is due to the  $\text{C}-\text{H}$  bending vibration. From the FTIR spectra, it may be concluded that oleate anion has been intercalated successfully into the gallery of the LDH.

The thermal stabilities of ZnAl–Oleate LDH and MgAl–Oleate LDH were analyzed in TGA experiments, in air, and the TGA curves are shown in Figs. 3 and 4. For ZnAl, the onset temperature (defined herein as the temperature at which 10% mass loss occurs) is  $248^\circ\text{C}$ , and the temperature of 50% mass loss is  $478^\circ\text{C}$ , both of which are higher than those of MgAlO-LDH; the values for MgAlO are  $219^\circ\text{C}$  and  $358^\circ\text{C}$  for 10% and 50% mass loss, respectively. There is a much larger residue for ZnAl than for MgAl since the inorganic content is higher due to the higher atomic weight of zinc; the residue values are 38.2% and 25.5%, respectively. The degradation of an LDH occurs typically in three steps which may overlap; these are 1) loss of water, 2) dehydroxylation, and 3)

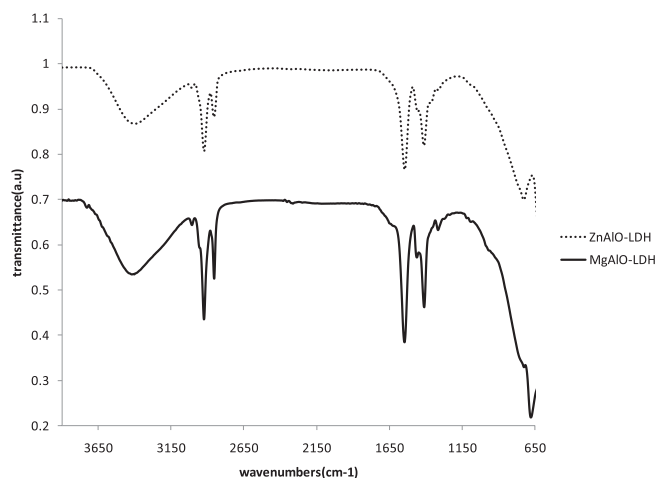


Fig. 2. FTIR spectra of MgAlO and ZnAlO LDHs.

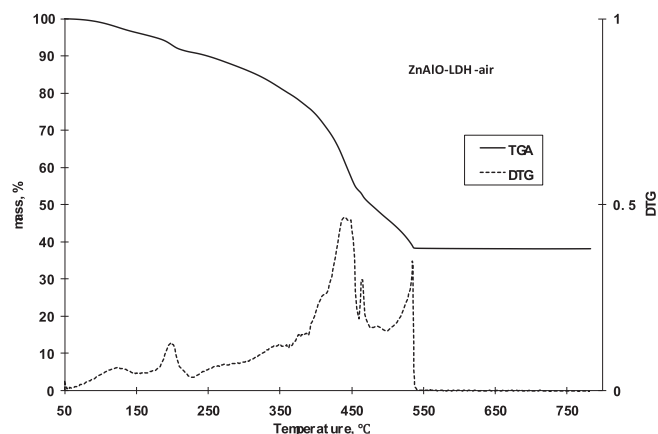


Fig. 3. TGA and DTG of ZnAlO-LDHX.

degradation of the organic species; the last two processes frequently overlap to some extent. From the DTG curves, one can observe essentially two steps in the degradation, loss of water below  $250^\circ\text{C}$  and loss of organics combined with dehydroxylation between  $250$  and  $550^\circ\text{C}$ . The residue which remains is a mixture of oxides and spinels, the exact composition depends somewhat on the identity of the metals [8g].

### 3.2. Morphology of the EVA/LDH composites

#### 3.2.1. The influence of LDH loading on the XRD and TEM

The XRD patterns of the EVA/LDH composites are shown in Figs. 5 and 6. For EVA–ZnAlO LDH at 3% LDH loading, the d-spacing is  $2.69\text{ nm}$  (this is actually smaller than the value recorded for the ZnAlO LDH, which is surprising despite the fact that both diffraction peaks are broad). Since the insertion of polymer into the gallery space of the LDH is typically accompanied by an increase in the basal spacing of the LDH, this XRD is indicative of an immiscible composite, although swelling of the LDH layers accompanied by loss of parallel registry cannot be excluded and may well be responsible for the rise of the background intensity seen at the lowest  $2\theta$  angles. As the loading of the LDH increases, the d-spacing decreases which is what one might expect, since an increase in loading makes dispersion more difficult; at 5% LDH the d-spacing is  $2.54\text{ nm}$  and at 10% it is  $2.52\text{ nm}$ . For MgAlO, the d-spacing is  $2.72\text{ nm}$  at 3% loading,  $2.54\text{ nm}$  at 5%

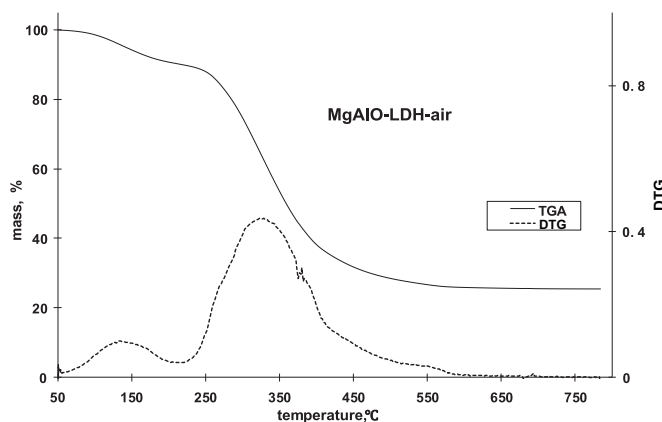


Fig. 4. TGA and DTG of MgAlO-LDH.

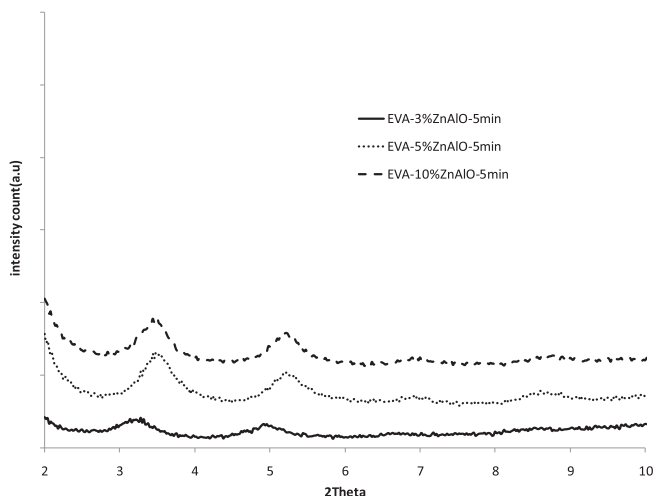


Fig. 5. XRD traces of EVA/ZnAlO-LDH composites at 5 min time for melt blending.

loading and 2.42 nm at 10% loading. These, once again, are all smaller than the d-spacing in the organically-modified LDH, but the decrease is not as large as what is seen for ZnAlO. Based only on XRD, one must assert that these systems are very likely to be microcomposites.

The effect of time of blending is shown in Figs. 7 and 8. With MgAlO, at 5 min blending time, the  $2\theta$  position is a little smaller than at other times; the position is essentially constant at other blending times and a slightly increased d-spacing, less than Å, is seen. Since the d-spacing at 1 min is the same as that at 15 min, one may conclude that time of melt blending has no effect on the morphology. For ZnAlO, the diffraction peaks either disappear or move to lower d-spacing *i.e.*, higher values of  $2\theta$ . The breadth of the peaks is indicative of disordering; this could either indicate a disordered microcomposite or an exfoliation type of disordering. Transmission electron microscopy is required to resolve this issue.

In order to better understand the morphology of a (nano) composite, one must also have information from transmission electron microscopy (TEM), or a similar technique that provides direct imaging of the morphology [11]. XRD investigations can only definitively detect periodic packings of layers at the nano-scale, whereas TEM permits the imaging of the actual clay layers

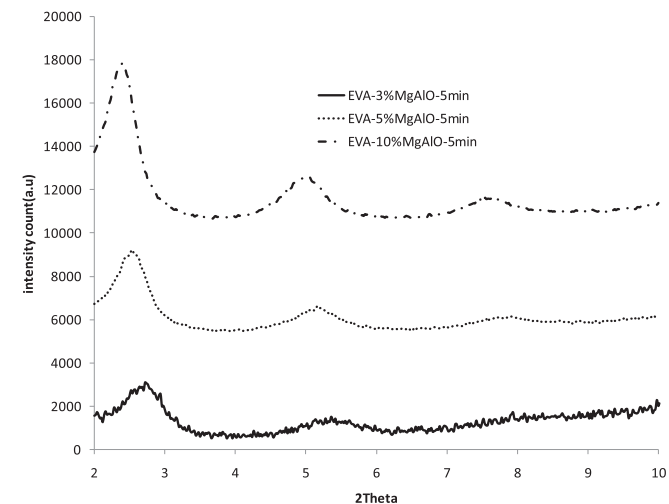


Fig. 6. XRD traces of EVA/MgAlO-LDH composites at 5 min time for melt blending.

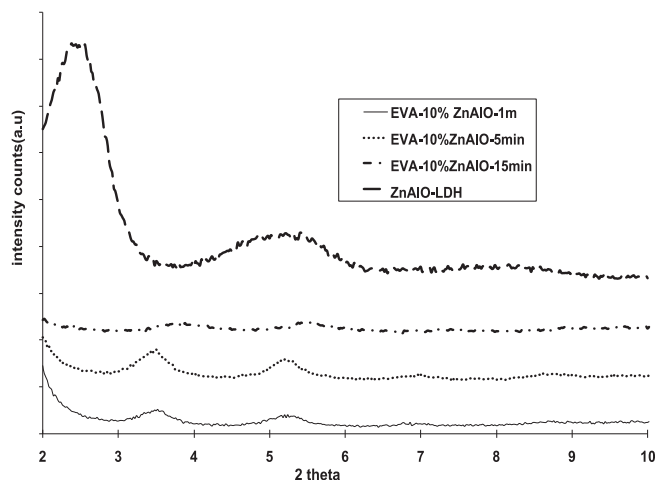


Fig. 7. Effect on XRD trace for ZnAlO-EVA at various times of melt blending. The top trace is that of the LDH, and the time of melt blending increases from 1 min to 5 min–15 min for the lower curves.

and agglomerates over the micrometer and nanometer length scales; thus, one can fully describe the morphology of the system by combining the two methods [11]. Despite imaging relatively small sample regions, representative TEM images at low magnification (which will show the global dispersion of LDH layers and will permit quantification of the material dispersion at the micrometer/agglomerate scale) and at higher magnification (which can show the actual individual nanoparticle fillers and, thus, permit assessment of the nanoscale filler dispersion, *viz.* assessment of whether the system is intercalated or exfoliated or, more likely, a mixture of these two morphologies) are used and considered to be representative of the composite. The TEM images of MgAlO in EVA at 5% loading are shown at various magnifications in Fig. 9. One can see in the low magnification image that the dispersion of LDH fillers is not very good and that there exist LDH layer assemblies throughout the EVA matrix, a typical morphology of a conventional composite (microcomposite). Higher magnification images, highlighting the composite structure at the tactoid length scale, show that the tactoids are swollen by the EVA matrix,

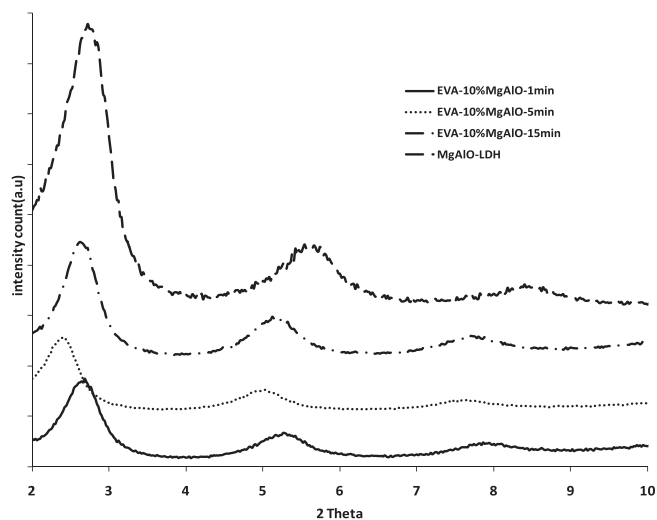
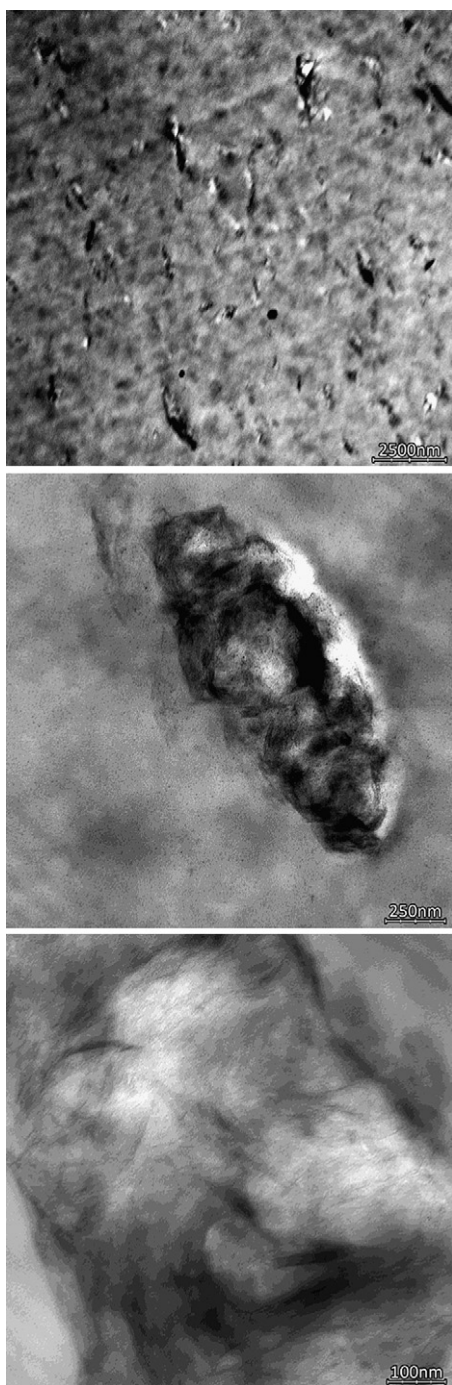
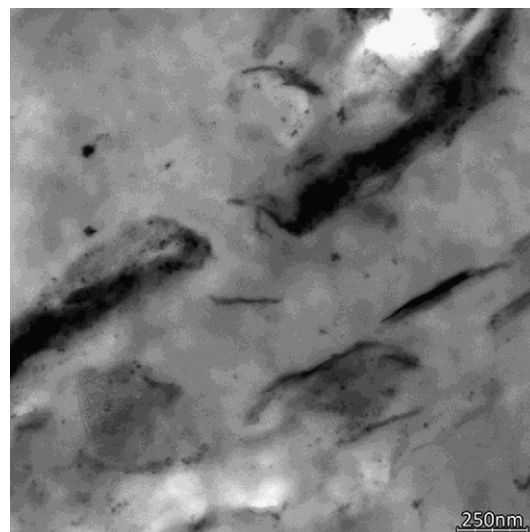


Fig. 8. Effect on the XRD trace for MgAlO-EVA at various times of melt blending. The top trace is that of the LDH, and the time of melt blending increases from 1 min to 5 min–15 min for the lower curves.



**Fig. 9.** Hierarchical composite morphology of EVA with 5% MgAlO. TEM images at: low magnification (top, highlighting the micrometer scale dispersion of filler assemblies), medium magnification (middle, showing the LDH tactoid structure as swollen by EVA), and higher magnification (bottom, showing the dispersion of individual LDH layers at the nanoscale).

and at an even higher magnification shows that the individual LDH clay layers are well-dispersed at the nanometer scale also showing periodic stacks of LDH layers that can give rise to a 003 diffraction peak. This hierarchical structure is rather typical of LDH-filled polymer composites, and can be summarily assigned as a microcomposite structure, and is also in accord with the XRD traces, in which the d-spacing of the composite was quantified to be slightly lower than that of the MgAlO LDH organofiller. When



**Fig. 10.** A TEM image of MgAlO at 10% loading in EVA highlighting the composite morphology at the tactoids length scale.

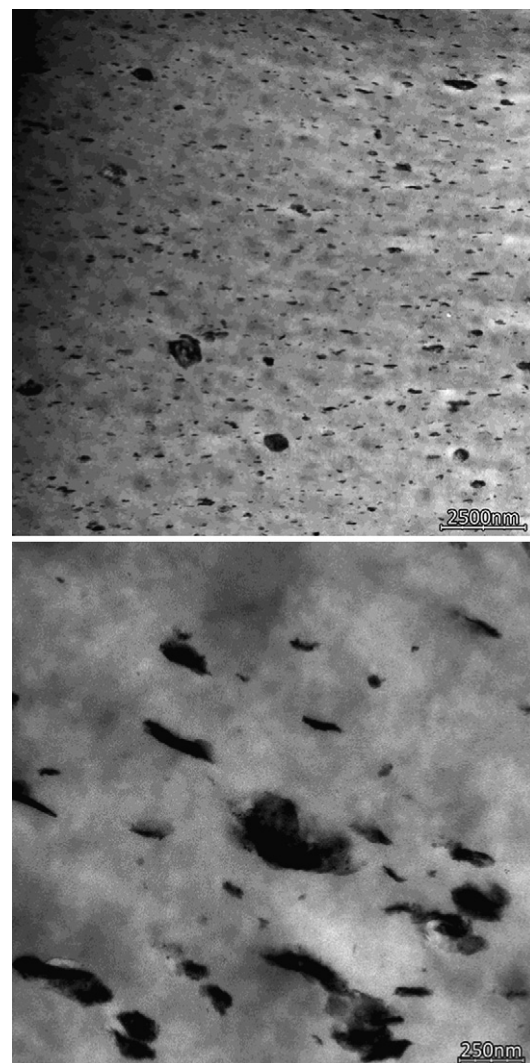


**Fig. 11.** Low magnification images of ZnAlO in EVA at 10% loading highlighting the dispersion at the micrometer scale and the tactoids' size. Compared to the MgAlO these composites show tactoids which are much smaller (better dispersion at the micrometer scale) but much more compact (less swollen by EVA, indicating worse nanometer scale dispersion).

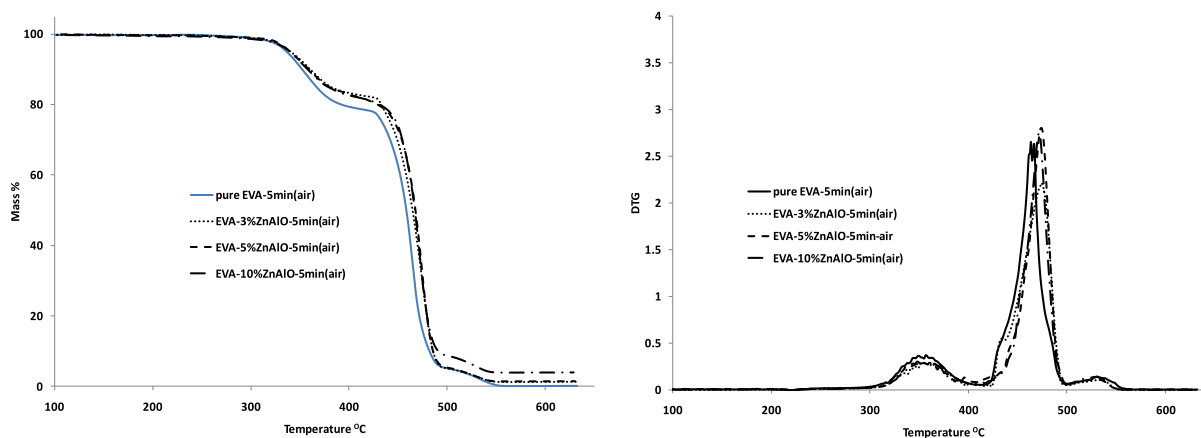


Fig. 12. TGA and DTG curves for EVA and its composites with ZnAlO-LDH.

the loading of MgAlO increases to 10%, the dispersion is not expected to be significantly different [12] and it is not. This system is also a microcomposite, with similar structure as that of the 5% MgAlO-EVA composite, and only one TEM image is shown in Fig. 10 highlighting the composite's morphology at the tactoids length scale.

For ZnAlO in EVA, once again the LDH dispersion is qualitatively the same as for the MgAlO (Fig. 11) and this system also exhibits a composite morphology consistent with a microcomposite structure. However, there are quantitative differences between the zinc-containing LDH and the magnesium-containing LDH composite morphologies. Specifically, compared to the magnesium-containing LDH composites the zinc-containing composites have 5–10 times smaller and more compact agglomerates; *i.e.*, the micrometer scale dispersion is better in the zinc-LDH composites, manifested in much finer tactoids, but these micron-sized LDH assemblies are less swollen by EVA polymer, indicating a poorer nanometer scale dispersion for the zinc-LDH (*cf.* Fig. 10 vs. Fig. 11).

These results are surprising and confusing. A MgAl LDH can be well-dispersed in poly(methyl methacrylate) (PMMA) while a ZnAl LDH is well-dispersed in non-polar polymers like polyethylene (PE) [8g]. We have yet to identify any compatibilizer that will permit good dispersion of an LDH in polystyrene (PS) [8] and it seems that EVA also falls into this category. More work must be done to

identify the various factors which control the dispersability of a nano-dimensional material in a polymer.

### 3.3. Thermal stability of the EVA composites

The TGA curves for EVA and its (nano)composites are shown in Figs. 12 and 13. The TGA curves show that when either MgAlO-LDH or ZnAlO-LDH are added to EVA, the thermal stability is enhanced. Thermal stability is evaluated using both  $T_{0.1}$ , the temperature at which 10% mass loss occurs, taken as a measure of the onset of the degradation, and  $T_{0.5}$ , the mid-point of the degradation, as well as the fraction of char which remains at the end of the degradation. From Tables 1 and 2, it can be seen that both degradation temperatures are increased compared to pristine EVA. Neither of these enhanced temperatures shows any marked dependence on either the amount or type of the LDH or on the time of melt blending.

#### 3.3.1. TGA–MS studies on the degradation of EVA and EVA-LDH nanocomposite

The degradation of EVA proceeds in two steps; the first step, which commences at about 300 °C involves the loss of acetic acid by a chain-stripping process and the second step, which begins above 400 °C is the degradation by a random scission process of the poly(ethylene-co-acetylene) polymer produced in the first

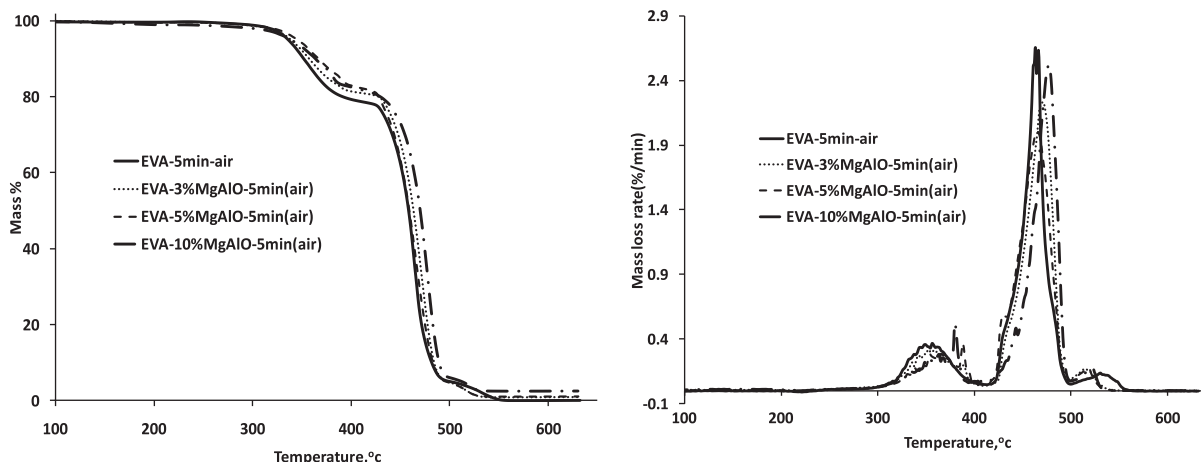


Fig. 13. TGA and DTG curves for EVA and its composites with MgAlO-LDH.

**Table 1**  
Summary of TGA data for EVA/ZnAlO-LDH in air.

Sample	$T_{0.1}$ (°C)	$T_{0.5}$ (°C)	%Residue	$\Delta T_{0.1}$	$\Delta T_{0.5}$
Pure EVA-1 min	348	451	0.0		
EVA-3%ZnAlO(2)-1 min	360	463	0.8	12	12
EVA-5%ZnAlO(4)-1 min	357	468	1.7	9	17
EVA-10%ZnAlO(5)-1 min	361	469	3.7	13	18
Pure EVA-5 min	352	458	0.1		
EVA-3%ZnAlO(2)-5 min	360	464	1.4	8	6
EVA-5%ZnAlO(4)-5 min	359	467	1.4	7	9
EVA-10%ZnAlO(5)-5 min	358	466	3.9	6	8
Pure EVA-15 min	350	461	0.7		
EVA-3%ZnAlO(2)-15 min	363	460	0.9	13	-1
EVA-5%ZnAlO(4)-15 min	357	464	2.2	7	4
EVA-10%ZnAlO(5)-15 min	356	464	4.9	6	4

Note: Indicated times denote process duration ("1 min" means melt blending for 1 min, etc.).

**Table 2**  
Summary of TGA data for EVA/MgAlO-LDH in air.

Sample	$T_{0.1}$ (°C)	$T_{0.5}$ (°C)	%Residue	$\Delta T_{0.1}$	$\Delta T_{0.5}$
Pure EVA-1 min	348	451	0.0		
EVA-3%MgAlO(2)-1 min	358	462	0.8	10	11
EVA-5%MgAlO(3)-1 min	356	459	1.2	8	8
EVA-10%MgAl(4)-1 min	363	466	2.5	14	15
Pure EVA-5 min air	352	458	0.9		
EVA-3%MgAlO(2)-5 min	357	463	0.9	5	5
EVA-5%MgAlO(3)-5 min	367	459	1.1	15	1
EVA-10%MgAl(4)-5 min	364	469	2.5	12	11
Pure EVA-15 min air	350	461	0.7		
EVA-3%MgAlO(2)-15 min	359	458	0.7	9	-3
EVA-5%MgAlO(3)-15 min	360	463	1.4	10	2
EVA-10%MgAl(4)-15 min	363	464	2.6	13	3

Note: Indicated times denote process duration "1 min" means melt blending for 1 min, etc.

degradation [13,14]. In a previous study with EVA–MMT nanocomposites, it was shown that the products produced in the second step are a series of alkanes, terminal olefins and  $\alpha,\omega$ -dienes [3c]. The same products were seen for both EVA and its MMT nanocomposite but the intensities were different. The TGA–MS used in this study obtains mass spectra in various cycles and a cycle corresponds to approximately 20 °C. Thus, for instance, cycle 12 corresponds to a temperature range of about 210–230 °C, cycle 17, is 328–348 °C, and cycle 23 is 442–462 °C. Figs. 14 and 15 present the TGA trace along with the DTG and the total ion current for various cycles in which the mass spectra were

collected. The respective mass spectra that were obtained for these cycles are presented in Fig. 16.

There are rather significant differences in the first step between pristine EVA and its MgAl LDH nanocomposite. For pristine EVA, the mass spectrum at about 300 °C shows peaks at  $m/e$  30, 32, 42, 43, 44, 45 and 60 which may be assigned respectively to formaldehyde, methanol, ketene, acetaldehyde – H, carbon dioxide and/or acetaldehyde, ethanol – H, and acetic acid. The first four species are believed to occur through cleavage of the acetate chain rather than chain stripping of this chain while, of course, acetic acid is produced through the chain-stripping process. The literature suggests that chain stripping, *i.e.*, the simultaneous loss of acetate and a hydrogen atom with the evolution of acetic acid, is the exclusive degradation pathway for the thermal degradation of EVA in the first step. This work shows that side chain fragmentation is competitive and, in fact, based on the intensities of the compounds produced, side chain fragmentation is probably the dominant mechanism of thermal degradation in this first step. A possible scheme to describe the process of side chain fragmentation is shown in Fig. 17. The group of Marosi has also seen side chain degradation as an alternative route for the first step of thermal degradation of EVA [15].

In the case of the LDH nanocomposite, the  $m/z$  value of 60 is not important. At 300 °C, the compounds noted above as arising from side chain degradation are visible and they become more pronounced at 320 °C; finally at 350 °C one observes a small peak at 60 along with a peak at 58, but the peaks for side chain degradation are by far the most important. The  $m/z$  value of 58 grows at 370 °C while acetaldehyde is the dominant peak and formaldehyde and methanol have almost vanished. By 385 °C, the mass spectrum is almost devoid of any features. One may imagine that the evolution of the acetic acid may be consumed via reaction with the hydroxyls of the LDH but this does not explain the peak at  $m/z = 58$ . Another explanation arises from the work of Martinez, Huff and Barteau [16], who reported that some catalysts are able to convert acetic acid that is evolved in their presence into a variety of other products, including ketene, acetaldehyde, CO<sub>2</sub> and acetone. They propose a process by which two molecules of acetic acid are coupled to produce acetone,  $m/z = 58$ , liberating CO<sub>2</sub> and water. This ketonization reaction has been shown to occur on a variety of metal oxides, including alumina [17] and MgO [18]. In a poster presented at the European fire retardancy meeting in 2009, Stec and Hull also reported the formation of acetone from the thermal degradation of an EVA nanocomposite; this was characterized by infrared spectroscopy [19].

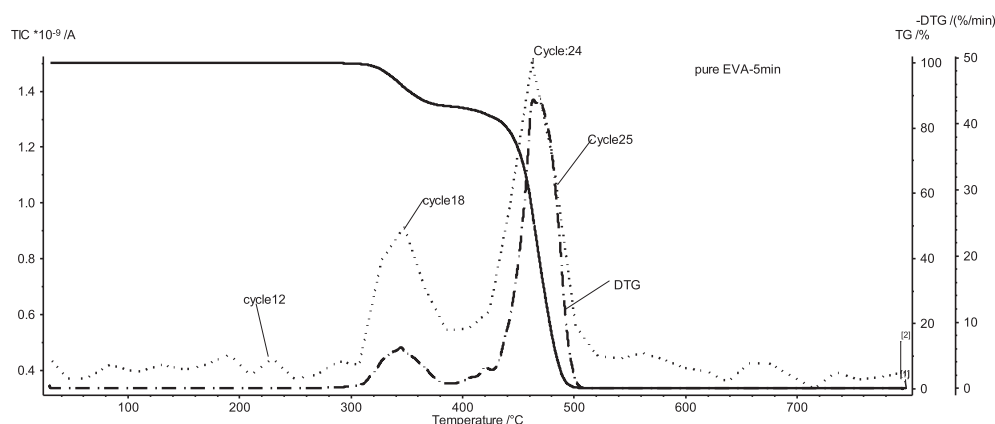


**Fig. 14.** TGA, DTG and total ion current for pure EVA.

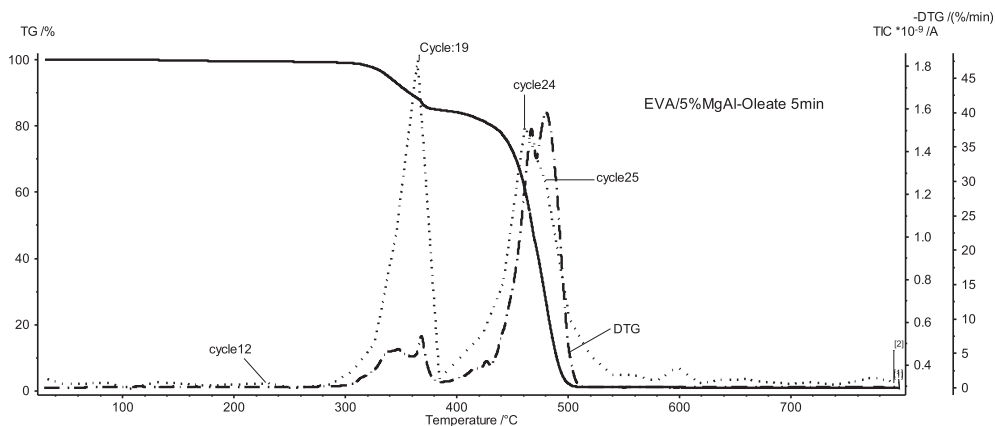


Fig. 15. TGA, DTG and total ion current for EVA/5%MgAlO-LDH.

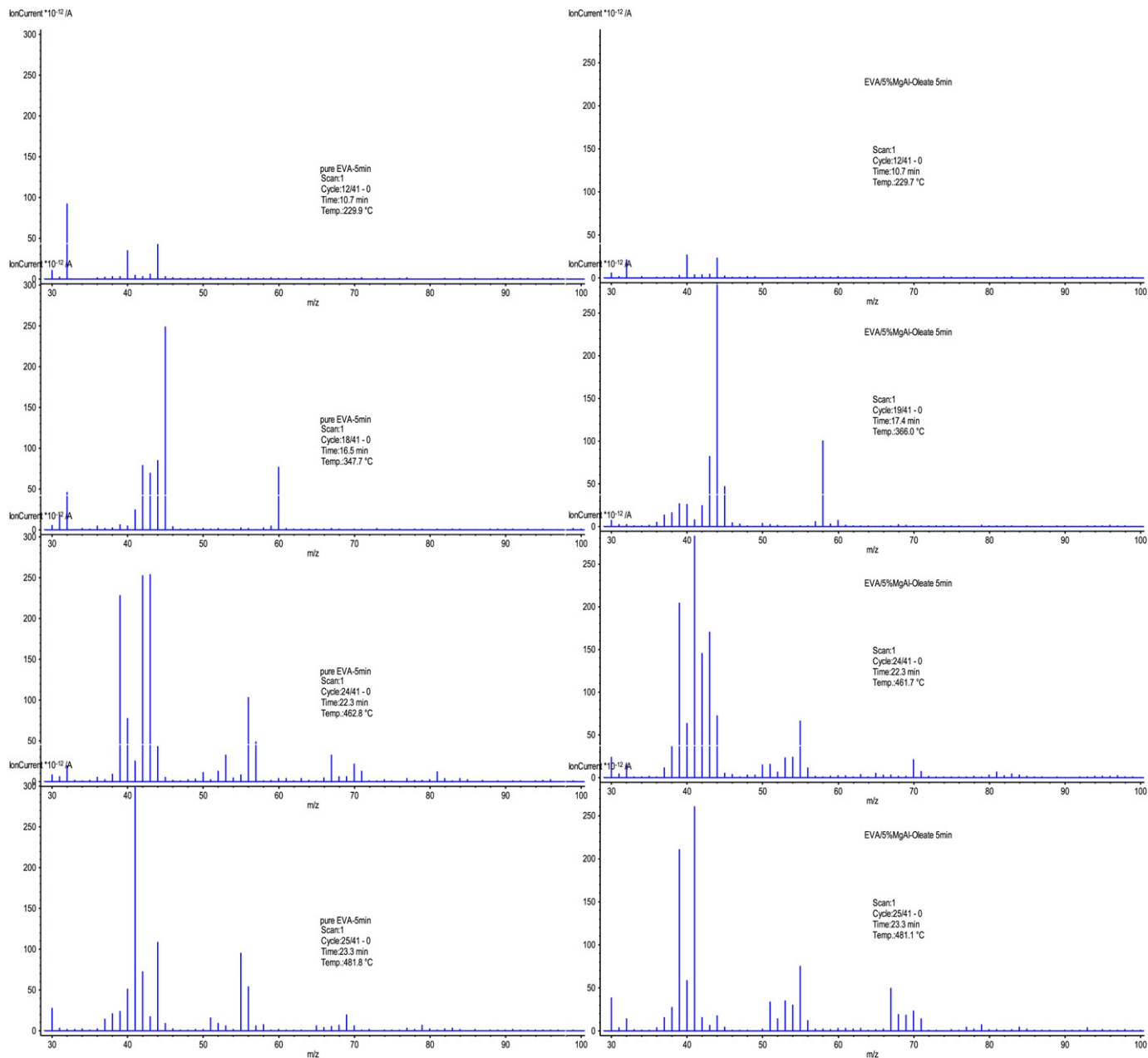


Fig. 16. Mass spectra for several temperature ranges in the degradation of both pristine EVA and its composites with 5% MgAlO.

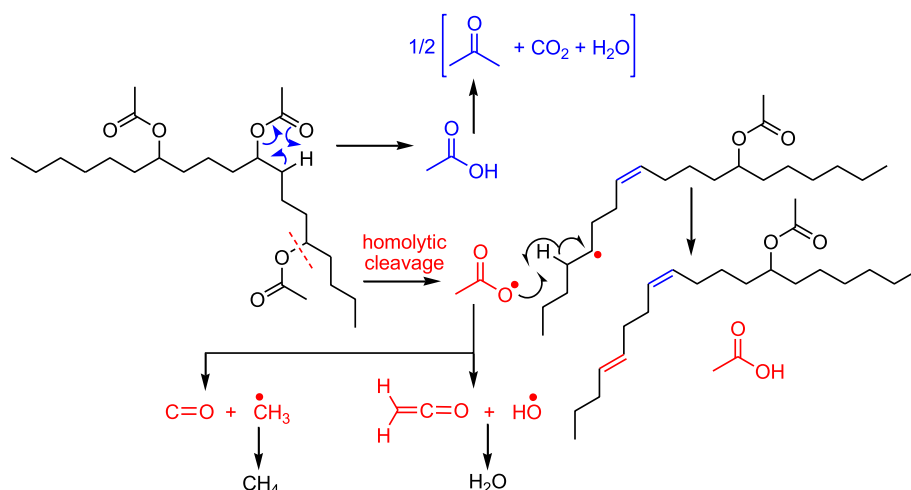


Fig. 17. A possible scheme to describe the process of side chain fragmentation in EVA.

The mass spectrometer that is connected to the TGA is functional to only about  $m/z$  of 100 and thus only low molecular weight species are observed in this study. In this sense, this complements previous work from these laboratories in which the degradation of EVA and its nanocomposites with MMT were studied by collecting the volatiles from the degradation and analyzing these by GC–MS; in that study the low molecular weight species are lost because they are quite volatile.

At 400 °C in pristine EVA one only observes three-carbon species, with the major peak in the mass spectrum assigned to  $C_3H_8$ . There is an additional peak at 43, due to the loss of H from propane, a small peak at 42 with a larger peak at 41 (loss of H), both assigned to  $C_3H_6$ . The most intense peak is due to propane, the least intense is that due to propene and the corresponding  $\alpha,\omega$ -diene, allene,  $C_3H_4$ , is of intermediate intensity. In the previous study of EVA degradation, three peaks were observed due to olefin, alkane and diene in that order of intensity. Here the same three peaks are seen but with a different intensity ordering. In the case of the LDH nanocomposite, peaks at 44, 43 and 42 are seen. These are assigned to propane, propane – H, and propene, respectively. Thus the presence of the LDH evidently increases the amount of olefin at the expense of the diene, exactly as seen for EVA–MMT nanocomposites.

At 420 °C in pristine EVA, propane and propene are the largest products with only a small amount of allene. For the first time, some C-4 products appear,  $C_4H_{10}$  and  $C_4H_8$ . The mass spectroscopic cross-sectional areas increase as the mass of the material increases [20] and thus, the large peaks for the lowest molecular weight materials do truly indicate that there is a preponderance of these low molecular weight materials. For the nanocomposite, the intensities change but the compounds do not. The C-3 compounds are still the dominant product but, interestingly, for propene, the peak at  $m/z$  42 is much more pronounced in the nanocomposite than in pristine EVA and the peak at  $m/z$  40, due to allene is also more intense. Apparently the presence of the LDH has an effect on the ease of loss of a hydrogen atom from hydrocarbon species. The only C-4 compound that is visible is at  $m/e$  58,  $C_4H_{10}$ , and again, in pristine EVA this appears at 57. There is less  $C_4H_{10}$  and more  $C_4H_8$  in the nanocomposite.

At 440 °C in pristine EVA, the most intense is  $C_3H_6$ , followed by  $C_3H_8$ , with  $C_3H_4$  being the least intense of the C-3 compounds. Likewise there is more  $C_4H_8$  than  $C_4H_{10}$  and only a very little  $C_4H_6$ . There are small amounts of higher homologues but their intensity is too low to be reliable. In the nanocomposite, there is more allene

than in pristine EVA. For the C-4 compounds, butene and butadiene are about equal in intensity, a rather different behavior from that in pristine EVA where the olefin was larger in intensity, and butane is essentially absent.

At 460 °C in pristine EVA, C-3 compounds still dominate and C-4 compounds are more intense, but now C-5 and even C-6 compounds can be observed. The C-3 alkane and alkene are about the same intensity while the diene is smaller. For C-4, the olefin is larger than the alkane and the diene is the smallest while for the C-5 species, the diene is largest in intensity followed by alkene with

Table 3

Mass spectrometric results from the TGA–MS study.

$m/z$	EVA, <230°	EVA/MgAlO, <230°	EVA, 328–405°	EVA/MgAlO, 328–405°	EVA, 442–500°	EVA/MgAlO, 442–500°
39	–	–	–	Sm	st	st
40	st	st	sm	Sm	st	st
41	–	–	sm	Sm	st	st
42	–	–	st	St	st	st
43	–	–	st	St	st	st
44	st	st	st	St	st	st
45	–	–	st	st	sm	sm
50	–	–	–	–	m	m
51	–	–	–	–	m	m
52	–	–	–	–	m	m
53	–	–	–	–	m	m
54	–	–	–	–	sm	m
55	–	–	–	–	st	st
56	–	–	–	–	st	m
57	–	–	–	sm	m	sm
58	–	–	–	st	–	–
59	–	–	sm	sm	–	–
60	–	–	st	sm	–	–
67	–	–	–	–	st	st
68	–	–	–	–	m	m
69	–	–	–	–	m	m
70	–	–	–	–	st	st
71	–	–	–	–	m	m
77	–	–	–	–	sm	sm
78	–	–	–	–	sm	sm
79	–	–	–	–	m	m
80	–	–	–	–	sm	sm
81	–	–	–	–	m	m
82	–	–	–	–	sm	sm
83	–	–	–	–	–	–
84	–	–	–	–	sm	sm

Note: “sm” is small; “m” is “medium”; “st” is “strong”.

**Table 4**  
cone results of EVA/LDH composites.

Formulation	PHRR Kw/m <sup>2</sup>	Reduct %	THR MJ/m <sup>2</sup>	ASEA m <sup>2</sup> /Kg	AMLR g/secm <sup>2</sup>	t <sub>ig</sub> sec	t <sub>PHRR</sub> sec
Pure EVA-1 min	1505 ± 87	NA	117 ± 0	292 ± 21	21.4 ± 0.1	65 ± 3	168 ± 4
EVA-3%MgAlO-1 min	1421 ± 3	6	117 ± 0	316 ± 52	17.6 ± 3.0	39 ± 8	166 ± 4
EVA-5%MgAlO-1 min	1357 ± 274	10	116 ± 0	351 ± 37	19.1 ± 2.0	44 ± 1	172 ± 8
EVA-10%MgAlO-1 min	1051 ± 73	30	115 ± 1	368 ± 41	18.1 ± 1.6	46 ± 5	173 ± 14
EVA-3%ZnAlO-1 min	1506 ± 30	0	118 ± 2	341 ± 40	20.6 ± 0.6	38 ± 8	155 ± 26
EVA-5%ZnAlO-1 min	1388 ± 33	8	117 ± 3	402 ± 33	19.2 ± 0.4	31 ± 1	155 ± 10
EVA-10%ZnAlO-1 min	1143 ± 88	24	115 ± 2	450 ± 26	18.9 ± 0.5	32 ± 6	160 ± 15
Pure EVA-5 min	1553 ± 27	NA	119 ± 1	274 ± 2	19.8 ± 0.3	64 ± 3	168 ± 1
EVA-3%MgAlO-5 min	1479 ± 78	5	118 ± 0	343 ± 15	19.9 ± 0.2	41 ± 7	167 ± 2
EVA-5%MgAlO-5 min	1392 ± 35	10	112 ± 3	387 ± 28	19.4 ± 0.5	47 ± 6	165 ± 14
EVA-10%MgAlO-5 min	988 ± 16	36	114 ± 1	436 ± 22	18.2 ± 0.1	49 ± 3	188 ± 16
EVA-3%ZnAlO-5 min	1472 ± 19	5	116 ± 3	332 ± 31	19.9 ± 0.1	46 ± 0	167 ± 12
EVA-5%ZnAlO-5 min	1409 ± 4	9	118 ± 2	388 ± 12	19.4 ± 0.1	36 ± 7	169 ± 8
EVA-10%ZnAlO-5 min	1191 ± 81	23	114 ± 2	410 ± 33	19.0 ± 0.3	32 ± 9	149 ± 6
Pure EVA-15 min	1467 ± 11	NA	113 ± 0	350 ± 25	20.4 ± 0.1	61 ± 1	168 ± 1
EVA-3%MgAlO-15 min	1325 ± 30	10	116 ± 1	389 ± 31	19.9 ± 0.3	46 ± 0	169 ± 6
EVA-5%MgAlO-15 min	1271 ± 139	13	113 ± 2	386 ± 41	19.5 ± 0.4	50 ± 2	174 ± 2
EVA-10%MgAlO-15 min	968 ± 14	34	112 ± 1	426 ± 23	17.6 ± 0.9	51 ± 2	180 ± 14
EVA-3%ZnAlO-15 min	1401 ± 68	4	114 ± 2	401 ± 65	21.6 ± 1.0	56 ± 8	169 ± 14
EVA-5%ZnAlO-15 min	1348 ± 72	8	111 ± 3	416 ± 4	20.2 ± 1.9	54 ± 6	163 ± 7
EVA-10%ZnAlO-15 min	990 ± 46	33	108 ± 1	468 ± 22	18.7 ± 0.6	45 ± 1	162 ± 9

alkane being the smallest. Only one C-6 species, at *m/z* 81 is observed; this should be assigned to C<sub>6</sub>H<sub>10</sub>. For the nanocomposite, the C-3 alkene is the largest followed by the alkane with the diene the smallest. For the C-4 family, the olefin is the largest and much bigger than the diene and the alkane which are about the same intensity. There is no C<sub>5</sub>H<sub>8</sub> detected and the C-5 alkene is larger than the alkane. Once again, only a small amount of C-6 species is detected but now both the alkane and the alkene are seen.

At 480 °C, there are significant differences between pristine EVA and its nanocomposite. In the pristine polymer, diene is much larger than alkane, which is in turn larger than alkene. In the nanocomposite, the olefin is the largest peak with the diene the smallest. For the C-4 family, in pristine EVA, olefin dominates while the amounts of alkane and diene are similar whereas for the nanocomposite, the olefin is still the largest but there is more diene than alkane. There is more C-5 alkene (with the loss of one hydrogen) than C<sub>4</sub>H<sub>10</sub> in pristine EVA and there is no C-6 material. In the nanocomposite, C<sub>5</sub>H<sub>10</sub> is the largest of the C-5 species but there is a small amount of the C-5 alkane. For C-6, small peaks at *m/z* 81 and 83 signify the presence of both the alkene and the alkane, both after loss of a hydrogen.

At 500 °C, one sees a reduced amount of all evolved materials but the C-3 materials are still dominant. For the C-3 compounds, the pristine EVA shows an order of alkane > diene > alkene, while in the nanocomposite the order is different: olefin > diene > alkane. For all other species, there are no apparent differences between the pristine EVA and the nanocomposite. At 520 °C, the results are very similar to those at 500 °C and only C-3 materials are evolved. All of the mass spectral data is collected in Table 3.

A summation of all of this data states that nanocomposite formation has a definitive effect on the degradation of the EVA and on the appearance of the species in the mass spectrum. However, this effect is not consistent. In previous work, it was found that less diene, less alkane and more olefin were produced in the degradation of the EVA nanocomposites than in pristine EVA, from looking at the larger materials that were evolved. Here it is found that the relative amounts depend on the length of the carbon chain, in some cases olefins are preferred and in other situations, other species become more dominant. It is very interesting that in some cases, the M-1 peak is observed while in other cases, the M peak is seen. Further study is necessary to systematically explore these effects.

#### 3.4. Fire retardancy of the EVA/MgAlO-LDH and EVA/ZnAlO-LDH composites

The cone calorimeter is the most effective method for laboratory evaluation of the fire properties of polymers. The parameters available from the cone calorimeter include: the heat release rate and especially its peak value (PHRR); the time to ignition (*t<sub>ig</sub>*) and the time to PHRR (*t<sub>PHRR</sub>*); the mass loss rate (AMLR); and the total heat released (THR). The ideal situation would be one in which the time to ignition is increased while the PHRR is greatly reduced and the THR also decreases, indicating that not all the polymer burns. Normally for nanocomposites, it is found that the reduction in the PHRR is due to the change in the mass loss rate, *i.e.*, the reduction in the loss of mass brings about a reduction in the heat which evolves. The data is collected in Table 4 and the heat release rate curves are shown in Figs. 18 and 19.

The data in Table 4 indicates that MgAlO is more effective in reducing the PHRR but it is only effective at 10% loading, at lower loading, either 3 or 5%, the PHRR is within the 10% error bars of pristine EVA. ZnAlO is as effective at 10% loading and 15 min mixing time as is MgAlO but this only occurs at 15 min of mixing. From XRD there is evidence of increased disorder at 15 min mixing time and the larger reduction in the PHRR could be attributed to better dispersion with the zinc-containing system at longer mixing times.

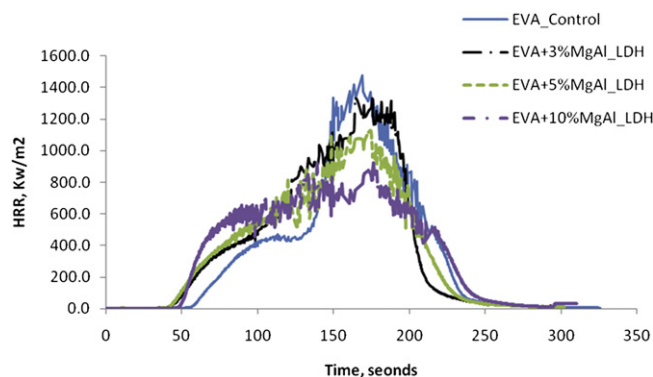


**Fig. 18.** Heat release rate curves for EVA and its composites with MgAlO.

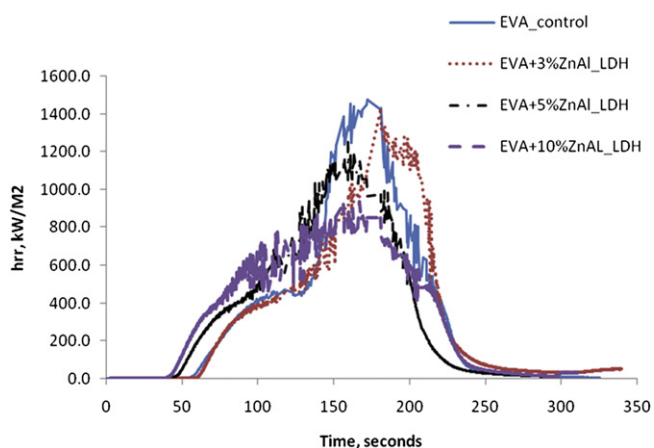


Fig. 19. Heat release rate curves for EVA and its composites with ZnAlO.

As is now unfortunately somewhat normal for polymer–clay nanocomposites, the results obtained from TEM, which examine only a very small portion of the material, and those from a bulk technique, like cone calorimetry, do not necessarily agree and this seems to be the case here. From the morphological investigation, the time of melt blending appears to have no effect on morphology but there is a larger reduction in the PHRR. At the moment, we can only acknowledge this difference and make efforts in the future to

resolve this. As is normal, the total heat released is virtually unchanged from pristine EVA to its composites, except for a small decrease due to the decreased amount of polymer. This is the normal situation with nanocomposites and indicates that all the polymer does burn. The change in mass loss rate is less than the change in PHRR, which likely indicates that some other process is involved in these systems. Since these systems are not well-dispersed on the nano-level, it is quite likely that more than simply a barrier effect, perhaps endothermic decomposition is also important in these systems. Once again, the time to ignition is seen to decrease, which is now known as typical behavior in the cone calorimeter when an additive is present.

Clearly, both LDHs are much less effective in reducing the peak heat release rate than is a montmorillonite, which typically gives a reduction of greater than 50% [3c,6]. One clear difference is in the dispersion, which is quite good for MMT and quite poor for an LDH. As has been shown previously, it is likely that the mechanism by which an LDH offers reduction in the PHRR is different from that operational for MMT [6]. Further work is necessary to identify these processes.

Pictures of the residue after the cone experiment can be useful for two reasons: 1) they show that when the clay is present in the polymer, dripping is suppressed and the sample maintains its shape and 2) the fraction of material which remains after the combustion can be seen. The images of the residues are shown in Fig. 20. Pristine EVA leaves no residue while for both the magnesium-containing and the zinc-containing LDH, residue is seen but it is only abundant at 10% loading. There is clearly more residue for

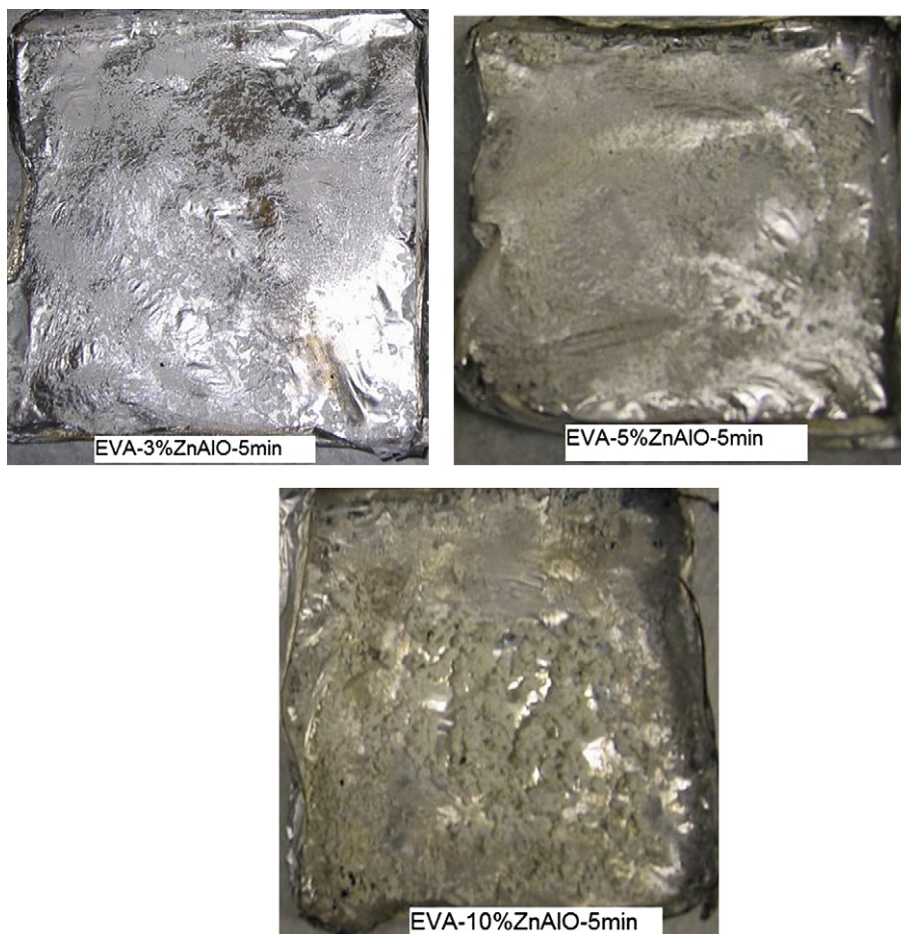


Fig. 20. Photographs of the cone residues.

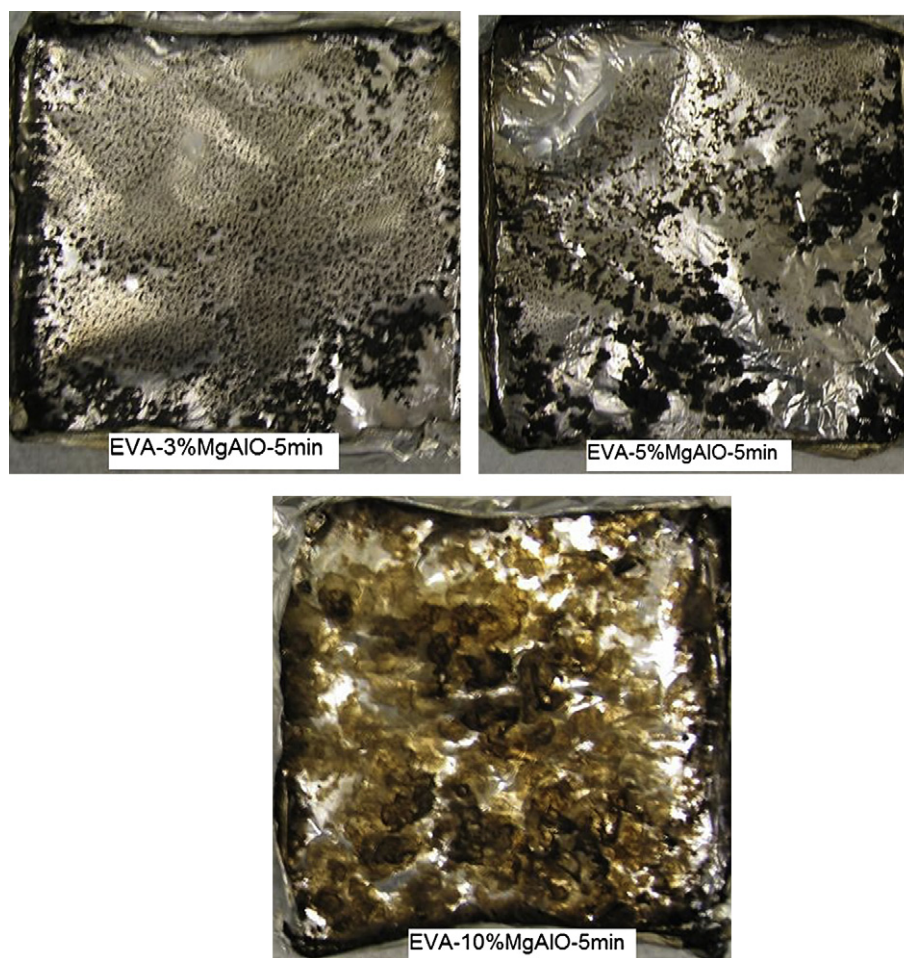


Fig. 20. (continued).

magnesium than for zinc but in neither case is the residue continuous and thus it is unlikely to offer very much protection.

#### 4. Conclusions

Melt blending of either a zinc-containing or a magnesium-containing layered double hydroxide with EVA results in micro-composites rather than genuine nanocomposites. These systems show enhanced thermal stability at all three loadings (3, 5 and 10%) that have been examined but they only show efficacy in fire retardancy at the highest (10%) loading. There is some evidence to suggest that better dispersion leads to a larger reduction in the peak heat release rate. From a TGA-MS study conducted at 5% loading of the magnesium-containing LDH, one can see that different products of degradation are obtained if one compares pristine EVA with the magnesium-containing LDH composite. The LDH evidently plays a significant role in the degradation of EVA. Two significant conclusions can be drawn from this work: 1) side chain fragmentation of the acetate group is not only competitive with chain stripping but may actually be the dominant mechanism and 2) the LDH plays a large role in the initial step of the degradation of EVA, in which for pristine EVA acetic acid is evolved but acetone, presumably produced due to catalysis by the LDH is evolved in the composite. More information is necessary to allow for a detailed interpretation of how these systems give enhanced fire retardancy.

#### References

- [1] Gilman JW, Jackson CL, Morgan AB, Harris Jr R, Manias E, Giannelis EP, et al. *Chem Mater* 2000;12:1866–73.
- [2] Chen K, Wilkie CA, Vyazovkin S. *J Phys Chem B* 2007;111:12685–92.
- [3] (a) Jang BN, Wilkie CA. *Polymer* 2005;46:2933–42; (b) Jang BN, Wilkie CA. *Polymer* 2005;46:3264–74; (c) Costache MC, Jiang DD, Wilkie CA. *Polymer* 2005;46:6947–58; (d) Jang BN, Wilkie CA. *Polymer* 2005;46:9702–13; (e) Jang BN, Costache M, Wilkie CA. *Polymer* 2005;46:10678–87.
- [4] (a) Kashiwagi T, Du F, Douglas JF, Winey KI, Harris Jr RH, Shields JR. *Nat Mater* 2005;4:928–33; (b) Kashiwagi T, Fagan J, Douglas JF, Yamamoto K, Heckert AN, Leigh SD, et al. *Polymer* 2007;48:4855–66; (c) Cipiriano BH, Kashiwagi T, Raghavan SR, Yang Y, Grulke EA, Yamamoto K, et al. *Polymer* 2004;48:6086–96.
- [5] Costache MC, Wang D, Heidecker MJ, Manias E, Wilkie CA. *Polym Adv Tech* 2006;17:272–80.
- [6] Costache MC, Heidecker MJ, Manias E, Camino G, Frache A, Beyer G, et al. *Polymer* 2007;48:6532–45.
- [7] Zammarano M, Bellayer S, Gilman JW, Franceschi M, Beyer FL, Harris RH, et al. *Polymer* 2006;47:652–62.
- [8] (a) Manzi-Nshuti C, Wang D, Hossenlopp JM, Wilkie CA. *J Mater Chem* 2008;18:3091–102; (b) Nyambo C, Songtipya P, Manias E, Jimenez-Gasco MM, Wilkie CA. *J Mater Chem* 2008;18:4827–38; (c) Nyambo C, Wang D, Wilkie CA. *Polym Adv Tech* 2009;20:332–40; (d) Wang LJ, Su S, Chen D, Wilkie CA. *Polym Degrad Stab* 2009;94:1110–8; (e) Nyambo C, Chen D, Su S, Wilkie CA. *Polym Degrad Stab* 2009;94:1290–7; (f) Nyambo C, Chen D, Su S, Wilkie CA. *Polym Degrad Stab* 2009;94:1298–306; (g) Manzi-Nshuti C, Songtipya P, Manias E, Jimenez-Gasco MM, Hossenlopp JM, Wilkie CA. *Polymer* 2009;50:3564–74.
- [9] Wang GA, Wang CC, Chen CY. *Polymer* 2005;46:5065–74.
- [10] Constantino VRL, Pinnavaia TJ. *Inorg Chem* 1995;34:883.

- [11] Morgan AB, Gilman JW. *J Appl Polym Sci* 2002;87:1329–38.
- [12] (a) Manias E. *Nat Mater* 2007;6:9–11;  
(b) Zhang JG, Manias E, Wilkie CA. *J Nanosci Nanotechnol* 2008;8:1597–615;  
(c) Dennis HR, Hunter DL, Chang D, Kim S, White JL, Cho JW, et al. *Polymer* 2001;42:9513;  
(d) Manias E, Touny A, Wu L, Strawhecker K, Lu B, Chung TC. *Chem Mater* 2001;13:3516–23;  
(e) Giannelis EP, Krishnamoorti R, Manias E. *Adv Polym Sci* 1999;138:107–47.
- [13] Cullis CF, Hirschler MM. *The combustion of organic polymers*. Oxford: Clarendon Press; 1981. p. 119.
- [14] Camino G, Sgobbi R, Colombier C, Scelza C. *Fire Mater* 2000;24:85–90.
- [15] Marosi G. private communication.
- [16] Martinez R, Huff MC, Barteau MA. *J Catal* 2004;222:404–9.
- [17] Pestman R, Koster RM, van Duijne A, Pieterse JAZ, Ponec V. *J Catal* 1997;168:265–72.
- [18] Sugiyama S, Sato K, Yamasaki S, Kawashiro K, Hayashi H. *Catal Lett* 1992;14:127–33.
- [19] Stec A and Hull TR. private communication.
- [20] Fitch WL, Sauter AD. *Anal Chem* 1983;55:832–5.